IEEE Access
Multidisciplinary | Rapid Review | Open Access Journal

Received October 10, 2019, accepted October 25, 2019, date of publication October 30, 2019, date of current version November 14, 2019.

Digital Object Identifier 10.1109/ACCESS.2019.2950521

Low-Profile Low-Cost Ultra-Wideband Circularly Polarized Slot Antennas

YONGSHENG PAN AND YUANDAN DONG, (Senior Member, IEEE)
School of Electronic Engineering, University of Electronic Science and Technology of China, Chengdu 611731, China
Corresponding author: Yuandan Dong (ydong@uestc.edu.cn)

ABSTRACT Aiming for ultra-wideband (UWB) indoor wireless access, three low-profile UWB circularly polarized slot antennas are proposed in this paper, all of which are made by a pair of curved tapered slots. The slots are miniaturized to allow a short direct microstrip feeding. The first antenna is a bidirectional antenna with a measured −10 dB impedance bandwidth of 110% (2.94 - 10.06 GHz), and a 3 dB axial ratio (AR) bandwidth of 89% (3.19 - 8.26 GHz). Its measured peak gain is 7.5 dBic and its size is 0.80 λ_{max} × 0.80 λ_{max} × 0.5 mm (λ_{max} is the free-space wavelength at the lowest frequency, 3.19 GHz). Its performance is similar to that of a traditional spiral antenna, but it has a much simpler structure with a more complete ground plane, making it possible to integrate with other components (e.g. filter and amplifier) on the antenna body to reduce the overall size of the system. The second antenna is a directional antenna with a simple solid metal reflector placed 21 mm away from the radiator. This configuration increases the peak gain to 8.6 dBic, but reduces the impedance bandwidth to 52% only. The third one is a directional antenna with a meshed reflector. It has a maximum gain of 9.6 dBic, which is higher than that of the second antenna, while its −10 dB impedance bandwidth is 99% (3.37 – 9.94 GHz) and its 3 dB AR bandwidth is 84% (3.70 - 9.07 GHz), which is similar to that of the first one. Also distance between the radiator and the reflector (antenna's height) is reduced to 9 mm only (0.111 λ_{max}). The proposed antennas demonstrate high efficiency, simple and low profile structures, wide impedance and AR bandwidth, making them excellent candidates for in-door base station and UWB positioning systems.

INDEX TERMS Circular polarization, metamaterial, printed antenna, slot antenna, ultra wideband (UWB) antenna.

I. INTRODUCTION

Ultra-wideband (UWB) positioning is most frequently used in applications such as in-door asset localization, personal tracking [1]. The wideband signal enables high precision positioning, making UWB popular for scenarios where accuracy of around 10 - 30 centimeters needs to be achieved. Antennas have a critical impact on its performance for UWB systems. Circularly polarized (CP) antennas have gained much attentions for its advantages in combating multi-path interferences and polarization mismatch losses [2].

Commonly used CP antennas, such as simple patch antennas, often have a narrow axial ratio (AR) bandwidth (e.g. less than 1%) [3]. In order to obtain wideband CP radiation, many structures have been investigated, such as the multi-feed [4], [5] and stacked [6] mircostrip patch antenna, wide-slot antenna [7]–[9], dielectric resonator antenna [10], single feed [11]–[14] and multi-feed [15] monopole and dipole antennas.

Among them the simplest way to achieve broadband CP operation is to use a spiral antenna, e.g. log-periodic spiral antenna [16]–[18], where its frequency-independent structure gives a good wideband feature. This kind of antenna can achieve an ultra-wide 3 dB AR bandwidth, e.g. 20:1, with a fairly simple structure. However, traditional spiral antennas need to wrap its arms for at least around one turn to get CP radiation, this make the metal part of the antenna more dispersed. These antennas usually require an additional differential feeding which is usually provided by a wideband balun [17].

By employing a novel slot shape, as shown in the left side of Fig. 1, we are proposing new wideband antennas with a more complete ground plane, which enables the integration of other components, and retained the broadband characteristic

The associate editor coordinating the review of this manuscript and approving it for publication was Chow-Yen-Desmond Sim.

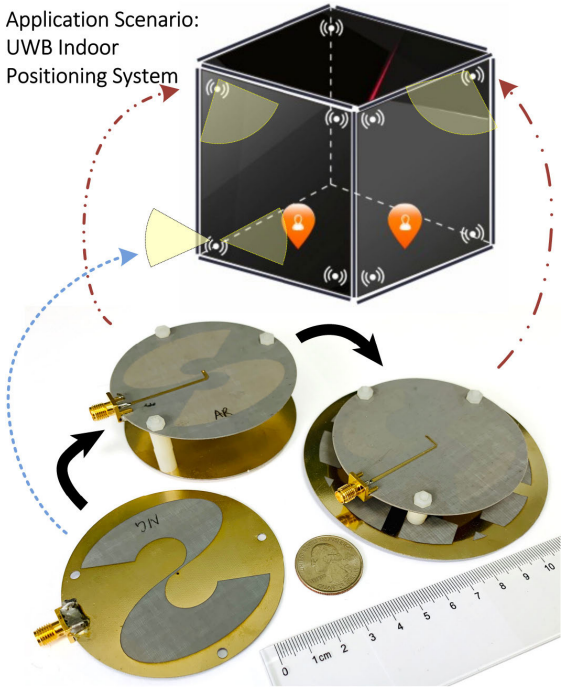

FIGURE 1. A photograph of the proposed antennas. Left side, bi-directional antenna; Upper side, directional antenna with solid metal reflector; Right side, directional antenna with meshed reflector; as well as an application diagram (top) as the in-door positioning anchor antenna.

of the traditional spiral antenna. Due to its reflectional symmetry structure, the radiation of this antenna (hereinafter ''bidirectional antenna'') is bidirectional.

In practical applications, directional antennas are also widely used, such as for the base stations on the ceiling. To meet this requirement, two directional antennas are proposed, the first of which has a simple solid reflector placed 21 mm away from the bidirectional antenna (that is around $\lambda/4$ of its center frequency). This antenna, hereinafter ''solid reflector antenna'', has a 1.1 dB increase in peak gain, but a narrower bandwidth compared to the bidirectional version.

For the other directional antenna, its reflector is changed into a meshed shape. This antenna, hereinafter ''meshed reflector antenna'', has a peak gain that is even 1 dB higher than that of the ''solid reflector antenna'', and a similar bandwidth as the ''bidirectional antenna''. Moreover, its height has been reduced to 9 mm, which is only 40% of that of the solid reflector antenna.

The following sections (Section II to IV) would detail the structure, principle, simulated and measured results for all of three antennas, respectively. Section V provides a comparison between three proposed antennas and other reported UWB CP antennas. A brief conclusion is drawn Section VI.

II. BIDIRECTIONAL UWB CP SLOT ANTENNA

A. ANTENNA CONFIGURATION

The structure and dimensions of the proposed bidirectional antenna are shown in Fig. 2 and Table. 1. This antenna

TABLE 1. Parameter list (unit: mm / deg).

R_1	R_2	R_3	R_4	R_5	W_1
15.1	27.3	8.0	9.3	37.5	1.3
L_1	L_2	T_0	θ_1	θ_2	
7.3	5.0	0.5	62.1	12.9	

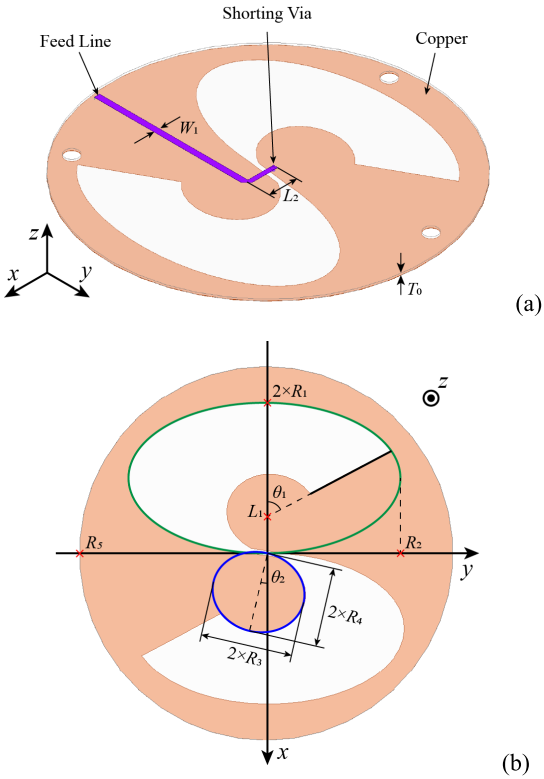

FIGURE 2. Structure of the proposed bidirectional antenna. (a) 3D view, and (b) Top view and dimensions of the antenna.

consists of two curved slots etched on the bottom layer of the PCB. The slot is obtained by cutting a bigger ellipse with a smaller rotated ellipse. Additionally, we cut its edge with a straight line to leave more space to the ground plane. The lowest end of two ellipses coincides with the center of the antenna, and the smaller ellipse is clockwise rotated along its lowest end by θ_2. To leave a gap of reasonable width at the junction of the two slots, a tiny rectangular slot with a width of 1 mm and a rotated angle of $\theta_2/2$ is placed at the center of the bottom layer.

The antenna is fed by an ''infinite balun'' which is initially mentioned in [16]. The structure is a microstrip line printed on the top layer of the PCB. It connects to the other side of the antenna's slot through a metalized via. The feedline is connected to the external equipment through a 3.5 mm 50 Ω SMA connecter.

The substrate of the PCB is F4BME220, with a thickness of 0.5 mm. This material's nominal performance is mostly the same as that of Rogers RO5880. Copper on the PCB is 1 oz (per square feet) thick. Its surface is gold plated to prevent oxidation.

B. OPERATING PRINCIPLE

Slots are fed by an ''infinite balun''. Instead of a quarter-wavelength matching stub, a shorting pin is directly employed providing a frequency independent matching/ connection to the antenna. It converts the current flow caused by the unbalanced microstrip feeding line gradually to the antenna radiation with negligible reflection. Current on the microstrip and ground caused by the unbalanced feeding from the SMA connector becomes balanced on the two edges of the slot after the shorting pin. And the tapered slot gradually converts the impedance from 50ohm to air impedance for radiation. The power is radiating fast while propagating along the tapered slot line. The feeding structure outside the antenna, e.g. coaxial line connected to the signal source, would barely impact the antenna radiation characteristic. This structure is essentially a direct connection and is frequency independent, providing a broadband matching and balun function.

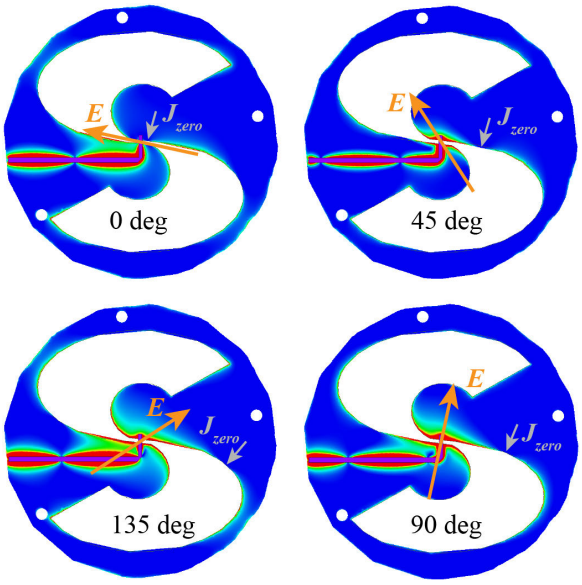

FIGURE 3. Simulated surface current density vs phase at 5 GHz.

Surface current on the ground plane and the direction of the radiated E field at different phase is shown in Fig. 3. As shown, the ''infinite balun'' successfully generates a traveling surface current on the edge of the slot. This current is traveling clockwise with the phase variation, thus will generate an E field rotating clockwise, which means the radiation along the +Z direction is LHCP.

The slot is acting as a slot transmission line, with a propagation mode similar to Quasi-TEM mode. The shorting end of the slot transmission line would cause reflection and generate standing wave. The reason why the traveling wave is generated instead of a standing wave is because the power is radiating fast enough, that the forward wave has decayed sufficiently before it propagates to the shorting end of the slot. So, the magnitude of the wave that is reflected by the shorting end of the slot is neglectable. Therefore, surface current in the format of ''traveling wave'' can be observed, which gives rise to the wideband characteristics of the proposed antenna. The upper limit of AR bandwidth is mainly determined by the shape of the slot. At high frequencies the wave is dissipating so fast that the main radiation happens before the slot bend sufficiently, making the radiation linearly polarized.

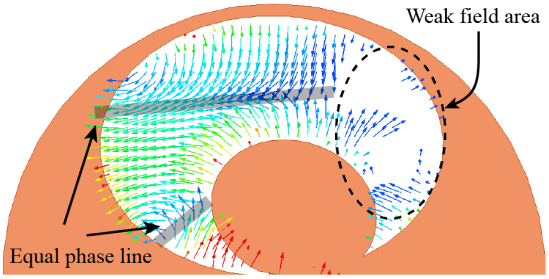

FIGURE 4. Simulated electric field at 5 GHz in the slot without the cutting.

In the original design, the slot was not cut by the straight line, as shown in Fig. 4. But simulation shows that the wave was not able to propagate along the slot to the outermost side, which generates a weak field area. As a result, the sharp corner of the slot was cut to leave more space to the ground. This provides the room for a simple microstrip feeding.

Dimensions such as R_1 to R_4 have a complex influence on the performance of this antenna. They not only impact the impedance matching but also the AR bandwidth. The final parameters of this antenna are determined with the help of the genetic algorithm integrated in ''Ansys Electronic desktop''.

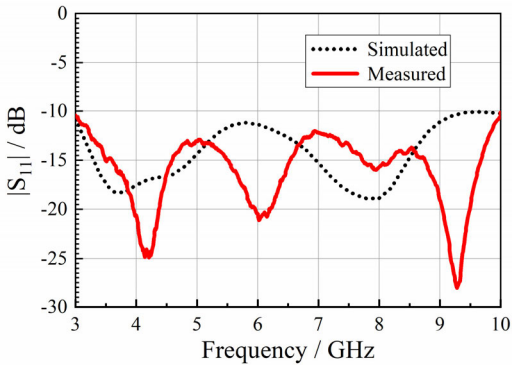

FIGURE 5. Simulated and measured $|S_{11}|$ of the proposed bidirectional antenna.

C. SIMULATED AND MEASURED RESULTS

Simulated and measured results of the proposed bidirectional antenna are shown in Figs. 5 to 8. Simulations in this paper are performed using Ansys HFSS. The impedance of the manufactured antenna is measured with Rohde-Schwarz ZNB40 network analyzer (100 kHz - 40 GHz), and the radiation character is measured with a far field antenna chamber and a Satimo Starlab Near-Filed measurement system (800 MHz - 6 GHz).

The measured 3 dB AR bandwidth is 89% (3.19 - 8.26 GHz), −10 dB $|S_{11}|$ bandwidth is 110% (2.94 - 10.06 GHz). Difference between the measured and simulated

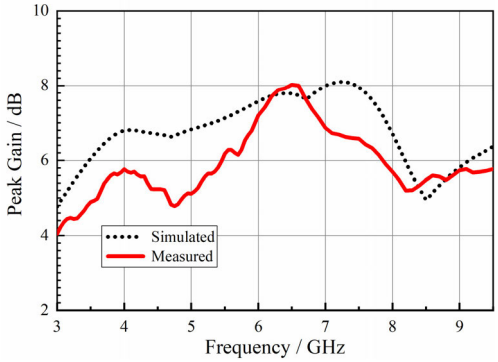

FIGURE 6. Simulated and measured peak gain of the proposed bidirectional antenna.

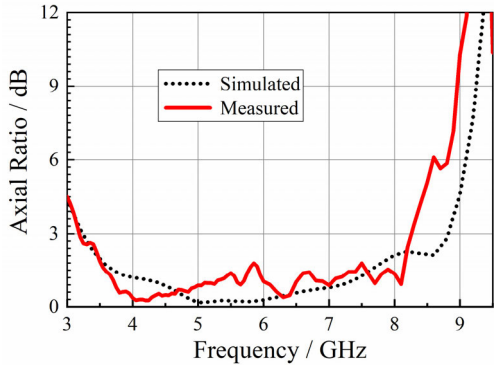

FIGURE 7. Simulated and measured axial ratio of the proposed bidirectional antenna.

$|S_{11}|$ is caused by the error introduced by the SMA connector and soldering. Its peak gain is 7.5 dBic. The lowest efficiency between 3 - 6 GHz is −0.9 dB (81.3%). Fig. 8 shows the realized gain and AR pattern of the proposed bidirectional antenna. As shown, the radiation of this antenna is LHCP along +Z direction and RHCP along −Z direction.

III. DIRECTIONAL SLOT ANTENNA WITH SOLID GROUND

To meet the requirement of directional radiation, a simple solid metal reflector is added to the bidirectional antenna.

A. ANTENNA CONFIGURATION

This antenna consists of a radiator, a reflector, and three sets of nylon screws for fixing purpose, as shown in Fig. 9. Radiator and reflector use the same PCB as the bidirectional antenna introduced in Section II, with the same R_5 and T_0. Other dimensions of the radiator are re-optimized for better performance, as shown in Table. 2. And the reflector is just a simple single-sided solid metal PCB without etching.

B. SIMULATED AND MEASURED RESULTS

Figs 10 to 13 show the simulated and measured performances of the proposed solid reflector directional antenna, including reflection coefficient, boresight gain, radiation efficiency, and radiation patterns. Fig. 11. shows that the peak gain of this

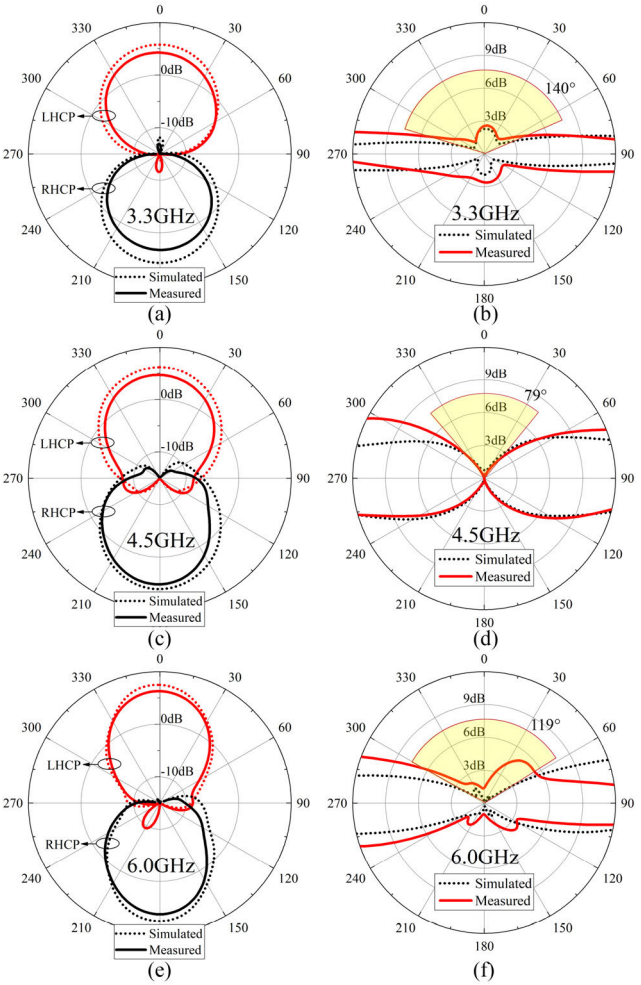

FIGURE 8. Simulated and measured far field patterns ($\varphi = 0°$). (a), (c) and (e) are realized gain patterns. (b), (d) and (f) are AR patterns at different frequencies.

TABLE 2. Parameter list (unit: mm / deg).

R_1	R_2	R_3	R_4	R_5	H
13.8	27.9	5.3	8.6	37.5	21
L_1	L_2	θ_1	θ_2	T_0	W_1
0.4	3.6	52.8	19	0.5	1.3

antenna is 8.6 dBic in-band, which is 1.1 dB more than the bidirectional one. Its efficiency is also good, better than −1 dB (80%) in band. As shown in Fig. 12, this antenna produces directional radiation. Measured highest back lobe level is less than −6.6 dB at 4.1 GHz.

However, the bandwidth of this antenna is considerably narrower than that of the bidirectional one. As shown in Fig. 10 and 13, measured impedance and AR bandwidth is only 52% (4.26 - 7.23 GHz) and 38% (3.95 - 5.80 GHz), respectively. This is due to the fact the phase of the reflected wave generated by the reflector is frequency dependent. For frequencies that are too far away from the center, the reflected wave would not be able to superpose with the wave generated by the radiator in-phase.

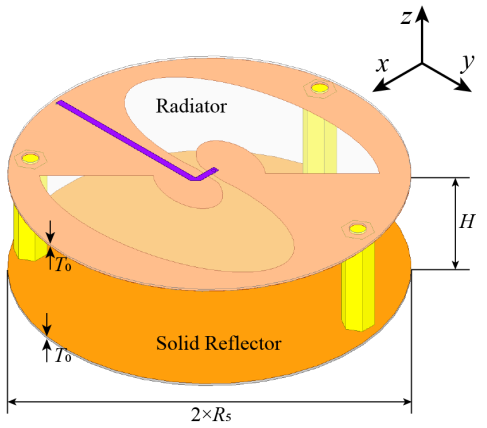

FIGURE 9. Structure of the proposed solid reflector antenna.

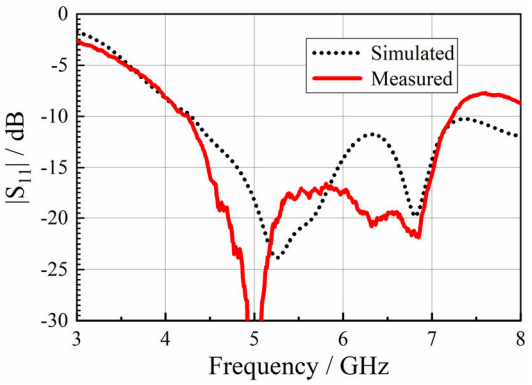

FIGURE 10. Measured and simulated $|S_{11}|$ of the proposed solid reflector antenna.

TABLE 3. Parameter list (unit: mm / deg).

R_1	R_2	R_3	R_4	R_5	R_6	L_1	L_2	H
14.7	26.2	9.6	11.4	37.5	49	9.5	4.5	9
θ_1	θ_2	θ_3	T_0	W_1	W_2	W_3	W_4	
42.4	18.2	31.8	0.5	1.3	0.83	6.1	17.3	

IV. DIRECTIONAL ANTENNA WITH MESHED GROUND

To solve the problem of narrow bandwidth and large height caused by the reflector. A meshed shape reflector is applied.

A. ANTENNA CONFIGURATION

Fig. 14. shows the structure of the proposed meshed reflector antenna. The antenna parameters are show in Table 3. This antenna has the same components as the solid reflector antenna mentioned in Section III, but with the reflector changed to a meshed metal. This mesh is printed on a single-sided PCB with a radius larger than the radiator. And the distance between the radiator and the reflector is 9 mm, only 40% of that of the solid reflector antenna (21 mm).

The microstrip line is also slightly adjusted, from a line of equal width to a tapered line, this can improve the impedance matching.

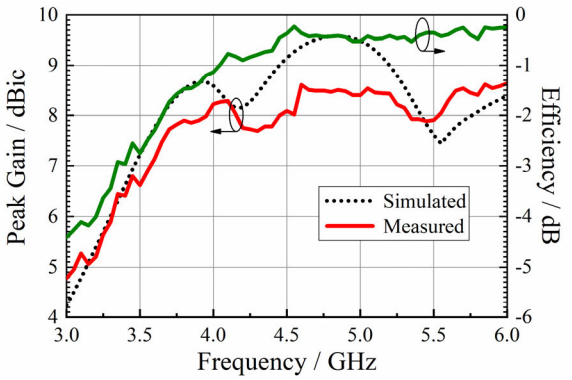

FIGURE 11. Measured and simulated peak gain and efficiency of the solid reflector antenna.

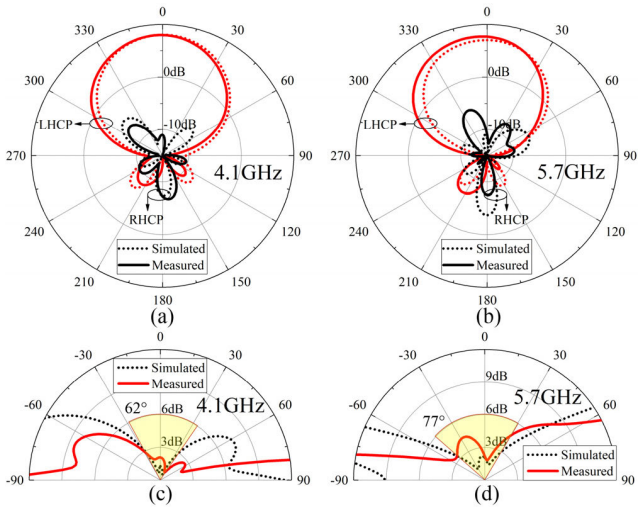

FIGURE 12. Simulated and measured far field patterns ($\varphi = 0°$). (a) and (b) are realized gain patterns. (c) and (d) are AR patterns at 4.1 GHz and 5.7 GHz.

B. OPERATING PRINCIPLE

This antenna is characterized by that it exhibits both wide bandwidth and directional radiation, but with a significantly lower height.

Its low-height feature comes from the shape of the reflector. For antennas using traditional metal plane reflector, in order to make the reflected wave and the original radiating energy sum up in phase, its reflector needs to be placed at least $\lambda/4$ away from the radiator. This distance provides a 180° phase delay for the reflected wave, so the total phase change will be 0° after considering the 180° phase advance introduced by the metal plane.

Here by using the mesh shape, the reflector, which is considered as a reactive impedance surface, could generate a phase advance smaller than 180°, as shown in Fig. 15. This is caused by the inductance introduced by the meshed reflector. According to [19]–[21], a metal strip array is capacitive when it is perpendicular to the E field, and inductive when it is parallel to the E field. And a mesh could be considered as a parallel LC resonant tank, as shown in Fig. 16. The value

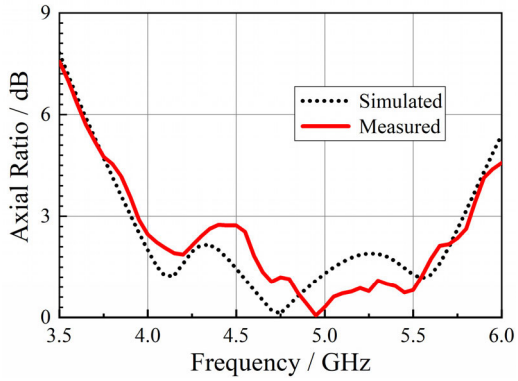

FIGURE 13. Simulated and measured axial ratio of the solid reflector antenna.

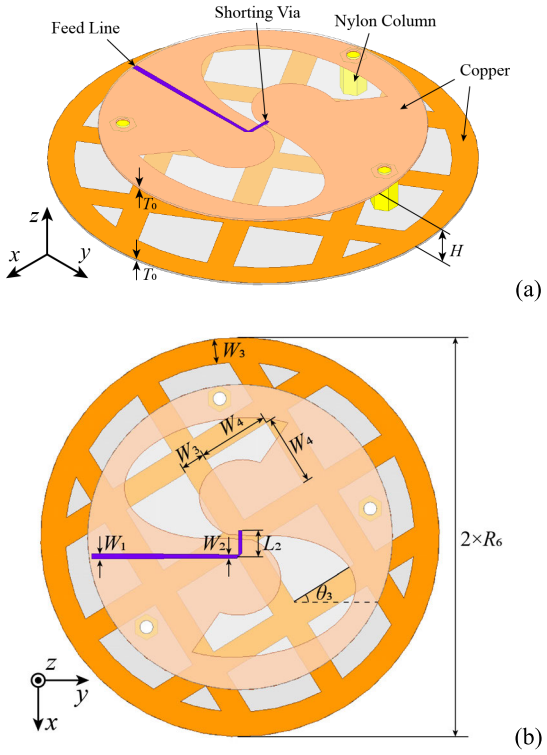

FIGURE 14. Structure of the proposed meshed reflector antenna, (a) perspective view, and (b) top view.

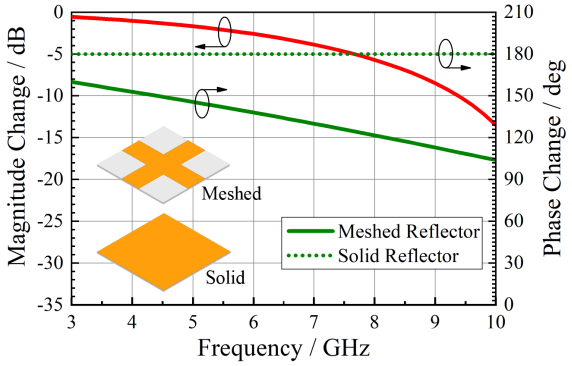

FIGURE 15. Simulated magnitude of reflected wave compared to the incident wave for an infinite mesh reflector (red line). And phase change for a solid metal reflector and a meshed reflector (green lines). And simulation model of solid and meshed reflector (ports are embedded to the reflector plane).

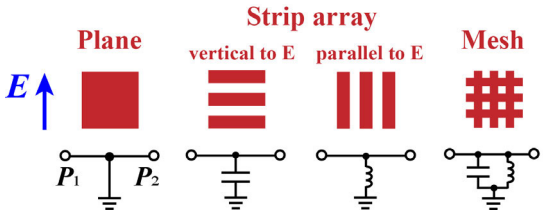

FIGURE 16. Equivalent circuit of metal plane, strip array, and meshed reflector.

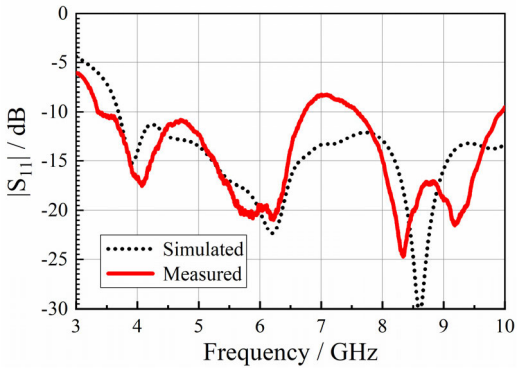

FIGURE 17. Simulated and measured $|S_{11}|$ for the meshed ground antenna.

of L and C could be roughly calculated with the following equations [19]:

$$L = \mu_0 \frac{(W_3 + W_4)}{2\pi} \log\left(\csc \frac{\pi W_3}{2(W_3 + W_4)}\right) \quad (1)$$

$$C = \epsilon_0 \frac{2(W_3 + W_4)}{\pi} \log\left(\csc \frac{\pi W_4}{2(W_3 + W_4)}\right) \quad (2)$$

where W_3 and W_4 represents the dimensions of the mesh as shown in Fig. 14.

As the operation frequency of this antenna is lower than the resonant frequency of the LC circuit, this mesh will be inductive, and will generate a phase advance smaller than 180°. So even if the phase delay provided by the distance between radiator and reflector is smaller than 180°, a total phase shift around 0° can be obtained. Therefore, the distance guided by a smaller phase delay between the radiator and the reflector, which is the height of the antenna, can be shortened.

Note that according to Fig. 15, the simulated phase change of the meshed reflector is only about 30° lower than the solid reflector at the minimum frequency. However, the height is changed from 21 mm to 9 mm, which means that the phase needs to be 100° lower. This difference is because the radiator is a slot, which has a relatively strong magnetic field in the near field region of the antenna. The orientation of the meshed ground is slightly tuned so that the opening direction of the mesh is along the similar direction of the slot, and the phase

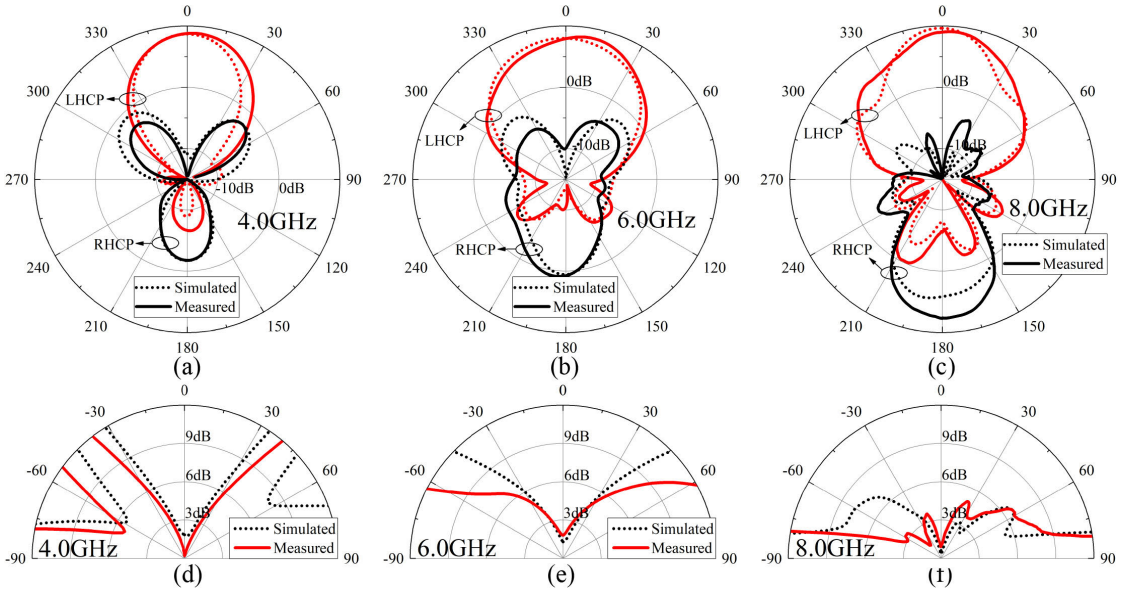

FIGURE 18. Simulated and measured far field patterns ($\varphi = 0°$). (a), (b) and (c) are realized gain patterns, while (d), (e) and (f) are AR patterns at 4, 5, 8 GHz.

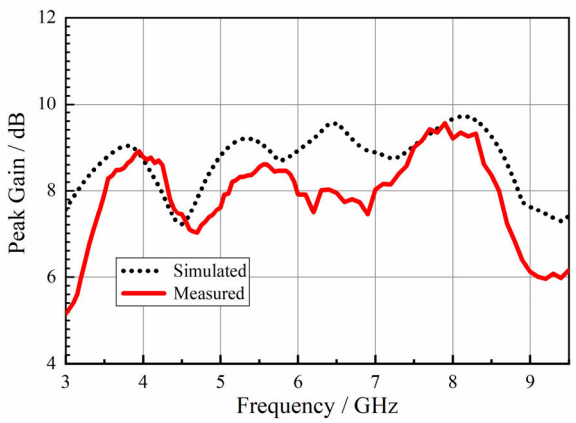

FIGURE 19. Simulated and measured peak gain of the meshed reflector antenna.

advanced introduced by the meshed ground actually is even smaller. The fields are interacting together which results in a smaller phase shift with a slightly different inductance at the same frequency.

Wideband feature of this antenna comes from its low height, and the frequency characteristic of the mesh reflector. The derivative of the phase as a function of frequency ($d\varphi/df$), is proportional to the propagation distance (l), that is:

$$d\varphi/df = 2\pi \times l/c \tag{3}$$

So, the shorter the propagation distance is, the less the phase changes with frequency, making the bandwidth wider. Another factor that widens the bandwidth is the energy leaked by the mesh reflector increases with the frequency, as shown in Fig. 15. This makes the characteristics of the antenna more similar to that of the bidirectional antenna at high frequencies. As shown in Fig. 18, the back lobe is becoming larger with the increase of the frequency.

C. SIMULATED AND MEASURED RESULTS

The simulated and measured results of the proposed meshed reflector antenna are shown in Figs. 17 to 20. As shown in Fig. 18, this antenna generates good directional radiation towards +Z direction, especially at lower frequency.

As shown in Figs. 17 and 20, this antenna exhibits broadband impedance and AR characteristics. Measured AR bandwidth is 84% (3.70 - 9.07 GHz). The measured results agree well with simulation. Most part of measured $|S_{11}|$ between 3.37 – 9.94 GHz (99%) is lower than −10 dB. Due to manufacture errors, $|S_{11}|$ is slightly higher than −10 dB at around 7 GHz. Measured efficiency between 3.70 – 6.0 GHz is all higher than −0.85 dB (82%).

V. COMPARISON

A comparison between three proposed antennas and other reported wideband CP antennas is provided in Table 3.

As shown, the three antennas proposed in this paper all exhibit a broadband characteristic. Among them, the bidirectional antenna has the widest impedance and AR bandwidth. For the solid reflector antenna, the introduction of the reflective surface increased the maximum gain by 1.1 dB, but significantly reduced the bandwidth. By switching the solid reflector to a mesh, the proposed "meshed reflector antenna" successfully expands the bandwidth to the same level of the bidirectional one, while still maintaining a high gain characteristic. The mesh also significantly reduces the antenna's height to 40% of the original level, from 0.298λ to 0.111λ.

Compared to [17] and [22] which also use the traveling wave structure, the proposed "meshed reflector antenna"

TABLE 4. Comparison between three proposed antennas and other wideband CP antennas.

	Radiator structure	Complexity	Antenna size with ground or cavity [1]	-10dB Impedance bandwidth	3dB AR bandwidth [2]	Peak Gain
Bidirectional (Proposed)	Curved slot	Simplest	75 × 75 × 0.5mm 0.80λ × 0.80λ × 0.5mm	2.94 - 10.06 GHz 110%	3.19-8.26 GHz 89%	7.5 dBic **(Bidirectional)**
Solid Reflector (Proposed)	Curved slot	Simple	75 × 75 × 21mm 1.07λ × 1.07λ × 0.298λ	4.26 - 7.23 GHz 52%	3.95-5.80 GHz 38%	8.6 dBic **(Directional)**
Meshed Reflector (Proposed)	Curved slot	Simple	98 × 98 × 9mm 1.21λ × 1.21λ × 0.111λ	≈ (3.37 – 9.94) GHz 99%	3.70 - 9.07 GHz 84%	9.6 dBic **(Directional)**
[17]	Inverted-S shaped metal strip (Balun feed)	Medium	90 × 90 × 18mm 1.2λ × 1.2λ × 0.24λ	3.4 - 6.5 GHz 63%	4 - 6.15 GHz 42%	≈10 dBic **(Directional)**
[22]	Cavity-backed aperture	Medium	30 × 30 × 10mm 0.98λ × 0.98λ × 0.33λ	9.8 - ≥13 GHz 28%	9.8 - 12.7 GHz 26%	≈8.5 dBic **(Directional)**
[23]	Crossed tapered slot (Dual feed)	Complex	53 × 53 × 48mm 0.33λ × 0.33λ × 0.3λ	1.85 - 6.24 GHz 109%	1.69 - 6.45 GHz 117%	8 dBic @5.5 GHz **(Directional)**

1. All λ is calculated according to the lowest frequency of the antenna.

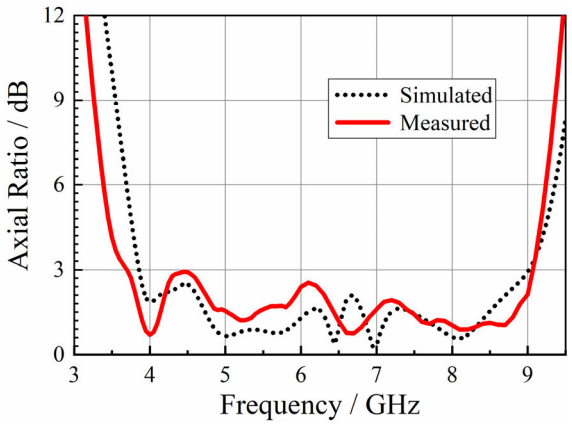

FIGURE 20. Simulated and measured axial ratio of the meshed reflector antenna.

achieved a much wider bandwidth and a similar directional gain, with a much lower height. Compared to [23] that use two crossed linearly polarized UWB antenna to achieve wideband CP radiation, the proposed antennas have a much simpler structure (only need two PCB and one welding), and a more stable gain (antenna gain of [23] drops by more than 3 dB below 3.5 GHz compared with the peak gain at 6 GHz). Compared to the balun configurations used in [17] and power divider used in [23], the feeding structure of the proposed antenna is only a simple microstrip line with a via. This reduces the loss and complexity of the feeding, and also facilitates the wideband operation.

Also, benefiting from the shape of the slot, the proposed antennas have a relatively complete ground plane near the feed point compared to other similar antennas, e.g. spiral antenna. This makes the proposed antennas insensitive under different environment. It also saves room for other circuits which could be integrated on the board.

VI. CONCLUSION

Three UWB CP slot antennas for in-door UWB positioning systems and other related applications are proposed in this paper, including the bidirectional antenna, the solid reflector antenna, and the meshed reflector antenna. Detailed discussion about the operating principles, and simulated/measured results for these antennas are provided sequentially in section II to IV (see Table. 4 for brief results).

By using a curved and miniaturized slot structure, these antennas realize the traveling wave operation mode, and thus exhibit a wideband characteristic. The ''infinite balun'' gives great simplicity and wideband features to the feeding structure. The meshed reflector structure helps to achieve a UWB directional CP radiation with a low-profile structure. And the shape of the slot also leaves a more complete ground plane which gives the possibility of integrating other components, e.g. filter or amplifier, on the antenna to save spaces for the whole system.

A simple comparison between three proposed antennas and other similar antenna are given in Section V. Results show that the proposed antennas exhibit desirable features of relatively low-profile, low-cost, large bandwidth, and simple structure, which make these antennas suitable for UWB wireless applications, such as in-door positioning systems.

REFERENCES

[1] S. Gezici, Z. Tian, G. B. Giannakis, H. Kobayashi, A. F. Molisch, H. V. Poor, and Z. Sahinoglu, ''Localization via ultra-wideband radios: A look at positioning aspects for future sensor networks,'' *IEEE Signal Process. Mag.*, vol. 22, no. 4, pp. 70–84, Jul. 2005.

[2] S. Gao, Q. Luo, and F. Zhu, *Circularly Polarized Antennas*. Hoboken, NJ, USA: Wiley, 2014.

[3] P. Sharma and K. Gupta, ''Analysis and optimized design of single feed circularly polarized microstrip antennas,'' *IEEE Trans. Antennas Propag.*, vol. AP-31, no. 6, pp. 949–955, Nov. 1983.

[4] S. D. Targonski and D. M. Pozar, ''Design of wideband circularly polarized aperture-coupled microstrip antennas,'' *IEEE Trans. Antennas Propag.*, vol. 41, no. 2, pp. 214–220, Feb. 1993.

[5] K.-L. Wong and T.-W. Chiou, "Broad-band single-patch circularly polarized microstrip antenna with dual capacitively coupled feeds," *IEEE Trans. Antennas Propag.*, vol. 49, no. 1, pp. 41–44, Jan. 2001.
[6] Nasimuddin, K. P. Esselle, and A. K. Verma, "Wideband circularly polarized stacked microstrip antennas," *IEEE Antennas Wireless Propag. Lett.*, vol. 6, pp. 21–24, 2007.
[7] H. Eskandari and M. N. Azarmanesh, "Bandwidth enhancement of a printed wide-slot antenna with a rotated slot," *Int. J. Electron. Commun.*, vol. 63, no. 10, pp. 896–900, 2009.
[8] K.-L. Wong, J.-Y. Wu, and C.-K. Wu, "A circularly polarized patch-loaded square-slot antenna," *Microw. Opt. Technol. Lett.*, vol. 23, no. 6, pp. 363–365, 1999.
[9] W. L. Chen, G. M. Wang, and C. X. Zhang, "Bandwidth enhancement of a microstrip-line-fed printed wide-slot antenna with a fractal-shaped slot," *IEEE Trans. Antennas Propag.*, vol. 57, no. 7, pp. 2176–2179, Jul. 2009.
[10] B. J. Xiang, S. Y. Zheng, Y. M. Pan, and Y. X. Li, "Wideband circularly polarized dielectric resonator antenna with bandpass filtering and wide harmonics suppression response," *IEEE Trans. Antennas Propag.*, vol. 65, no. 4, pp. 2096–2101, Apr. 2017.
[11] X. L. Bao and M. J. Ammann, "Printed circularly polarised antenna with ultra-wide axial-ratio bandwidth," *IET Microw., Antennas Propag.*, vol. 5, no. 9, p. 1089, 2011.
[12] H. Tang, K. Wang, R. Wu, C. Yu, J. Zhang, and X. Wang, "A novel broadband circularly polarized monopole antenna based on C-shaped radiator," *IEEE Antennas Wireless Propag. Lett.*, vol. 16, pp. 964–967, 2017.
[13] A. Panahi, X. L. Bao, G. Ruvio, and M. J. Ammann, "A printed triangular monopole with wideband circular polarization," *IEEE Trans. Antennas Propag.*, vol. 63, no. 1, pp. 415–418, Jan. 2015.
[14] K. G. Thomas and P. G, "A novel wideband circularly polarized printed antenna," *IEEE Trans. Antennas Propag.*, vol. 60, no. 12, pp. 5564–5570, Dec. 2012.
[15] J.-W. Baik, K.-J. Lee, W.-S. Yoon, T.-H. Lee, and Y.-S. Kim, "Circularly polarised printed crossed dipole antennas with broadband axial ratio," *Electron. Lett.*, vol. 44, no. 13, p. 785, 2008.
[16] J. D. Dyson, "The equiangular spiral antenna," *IRE Trans. Antennas Propag.*, vol. 7, no. 2, pp. 181–187, Apr. 1959.
[17] L. Zhang, S. Gao, Q. Luo, P. R. Young, W. Li, and Q. Li, "Inverted-S antenna with wideband circular polarization and wide axial ratio beamwidth," *IEEE Trans. Antennas Propag.*, vol. 65, no. 4, pp. 1740–1748, Apr. 2017.
[18] S. G. Mao, J. C. Yeh, and S. L. Chen, "Ultrawideband circularly polarized spiral antenna using integrated balun with application to time-domain target detection," *IEEE Trans. Antennas Propag.*, vol. 57, no. 7, pp. 1914–1920, Jul. 2009.
[19] S. Tretyakov, *Analytical Modeling in Applied Electromagnetics*. Norwood, MA, USA: Artech House, 2003.
[20] N. Marcuvitz, *Waveguide Handbook* (M.I.T. Radiation Laboratory Series), vol. 10. New York, NY, USA: McGraw-Hill, 1951.
[21] K. Sarabandi and N. Behdad, "A frequency selective surface with miniaturized elements," *IEEE Trans. Antennas Propag.*, vol. 55, no. 5, pp. 1239–1245, May 2007.
[22] K.-F. Hung and Y.-C. Lin, "Novel broadband circularly polarized cavity-backed aperture antenna with traveling wave excitation," *IEEE Trans. Antennas Propag.*, vol. 58, no. 1, pp. 35–42, Jan. 2010.
[23] X. Ding, Z. Zhao, Y. Yang, Z. Nie, and Q. H. Liu, "A compact unidirectional ultra-wideband circularly polarized antenna based on crossed tapered slot radiation elements," *IEEE Trans. Antennas Propag.*, vol. 66, no. 12, pp. 7353–7358, Dec. 2018.

YONGSHENG PAN received the B.S. degree in electrical engineering from the University of Electronic Science and Technology of China (UESTC), Chengdu, China, in 2018, where he is currently pursuing the M.S. degree. His research interests include miniaturized antennas, planar antennas and microwave devices for handset, and base station applications.

YUANDAN DONG (S'09–M'12–SM'16) received the B.S. and M.S. degrees from the Department of Radio Engineering, Southeast University, Nanjing, China, in 2006 and 2008, respectively, and the Ph.D. degree from the Department of Electrical Engineering, University of California at Los Angeles (UCLA), in 2012.

From September 2008 to June 2012, he was a Graduate Student Researcher with the Microwave Electronics Laboratory, UCLA. From September 2012 to February 2016, he was a Senior Engineer with the R&D Hardware Department, Qualcomm, San Diego. From February 2016 to December 2017, he was a Staff Engineer with Universal Electronics, Santa Ana. Since December 2017, he has been a Full Professor with the University of Electronic Science and Technology of China (UESTC). He has authored over 60 journal and conference papers. His research interests include the characterization and development of RF and microwave components, circuits, antennas, acoustic-wave filters, and metamaterials. He is serving as a Reviewer for several the IEEE and IET journals, including the IEEE TRANSACTIONS ON MICROWAVE THEORY AND TECHNIQUES and the IEEE TRANSACTION ON ANTENNAS AND PROPAGATION. He was a recipient of the Best Student Paper Award, in 2010 Asia Pacific Microwave Conference, Yokohama, Japan, the Distinguished Expert presented by Sichuan Province and by China Government, the High Level Innovative and Entrepreneurial Talent presented by Jiangsu Province.